Received: 25 September 2023 | Revised: 17 January 2024 | Accepted: 28 February 2024 | Published online: 29 February 2024

RESEARCH ARTICLE

Journal of Optics and Photonics Research
2025, Vol. 2(1) 45–53
DOI: 10.47852/bonviewJOPR42021793

BON VIEW PUBLISHING

Triple Micro Optical Multiple Asymmetric Ring Resonator Performance Analysis as Optical Filter

Shree Krishna Marandi[1], Kumari Sarwagya[2] and Suman Ranjan[1,*]

[1]*Birsa Institute of Technology Sindri, India*

[2]*Government Engineering College Arwal, India*

Abstract: This paper implements the modeling of triple asymmetrical optical microring resonator in z-domain, and the waveguide spacing is designed using finite difference time domain (FDTD) method. The formulation of the transmission function is prepared in z-domain utilizing the delay line signal processing technique. The developed configuration is scrutinized by evaluating the frequency response analysis as well as various important characteristics that are dispersion, group delay, and finesse using MATLAB software. The efficacy of the proposed methodology is tested using OptiFDTD software, and it is found that the results of both MATLAB and OptiFDTD are in very nearby settlement. The field analysis of propagated wave inside the microring resonator is shown. The specific gap for various optical directional couplers is also determined using OptiFDTD in this paper. The proposed technique is very useful for modeling and analyzing different configurations of micro optical asymmetric ring resonator which found great application in the field of optical filters as well as optical sensors.

Keywords: delay line, FDTD method, microring resonators, directional coupler

1. Introduction

Optical ring resonator is a fundamental component in the field of photonics and optical communication systems. It is a compact and versatile device that is widely used in various applications such as frequency division multiplexing [1], optical sensor [2, 3], optical switches [4], photonic biosensors [5], Brillouin ring laser gyroscope [6], optical spectral analyzer [7], etc. Triple asymmetrical optical microring resonators (TAOMRRs) are a type of optical filter that plays a crucial role in various applications within the field of photonics and optical communication. As communication technologies evolve, the demand for efficient high-capacity and flexible optical filters becomes increasingly highly important. The transmission functions of the developed configuration in the z-domain are determined using Mason's gain rule. Unit delay is used as a fundamental component of modeling, which is expressed as z^{-1}. The field investigation of the propagated wave is done using OptiFDTD software. The main purpose of the suggested work is to maximize ring resonator free spectral range (FSR) so that the specified filter will be suitable for different communication objective. MATLAB and OptiFDTD software is utilized for modeling a ring resonator mathematically in the z-domain, and its distinct properties were analyzed to monitor the performance of proposed filter. Finally, the MATLAB result is validated with the result obtained using OptiFDTD software, and it is observed that both the results are in very close agreement.

In 1995, Suzuki et al. [8] analyzed the performance of both single ring resonator and double ring resonator and it is found that the FSR of around 14.3 GHz and 98 GHz, respectively, is achieved. The z-domain correlation of fundamental optical circuits component utilized as filter was determined by Moslehi et al. [9]. The execution of the quadruple optical ring resonator is determined by using the delay line signal processing technique and the pentuple optical ring resonator with expanded FSR in order of terahertz [10, 11]. Yanagase et al. [12] presented vertical connected triple ring resonators with an increased FSR of 25.8 nm. Kokubun et al. [13] presented an approach for fabrication of a vertically connected microring resonator with a multilevel crossing bus line that may provide an FSR of about 5000 GHz (37 nm). With two asymmetrical ring radii and an FSR of 24 nm, Yan et al. [14] presented a 1 × 4 input–output configuration. Deng et al. [15] proposed an add-drop filter based on the microfiber knot resonator with an FSR of about 0.58 nm. Ahmed et al. [16] presented the corrosion sensing-based optical microring resonator with an FSR of about 40 nm.

Till now, many researchers have developed various configuration based on microring resonator for application as optical filter. The reported FSR in previously reported work suggests a requirement of expanded FSR. Also, none of the paper deals with the development of direction coupler, which is a huge research gap as directional coupler plays an important role in increasing the efficiency of the proposed structure. In this paper, the aforementioned gap is both studied and attempted to be addressed.

The proposed triple ring resonator has an excellent configuration that can improve the space utilization factor considerably, as well as increases the FSR, since two asymmetrical rings are housed inside a

*Corresponding author: Suman Ranjan, Birsa Institute of Technology Sindri, India. Email: sumanranjan.ee@bitsindri.ac.in

bigger ring, which requires less space compared to serially coupled rings. Smaller rings are accommodated within a larger ring, which contributes to extend the FSR as per Vernier principle, and the entire space required to fabricate the structure is restricted within the diameter of the larger ring. The directional coupler is designed using finite difference time domain (FDTD) technique by which exact waveguide spacings among different couplers can be estimated such that the overall efficiency of the proposed TAOMRR can be increased. The importance of TAOMRR lies in their unique design and performance characteristics, making them valuable components for optical filtering in communication system. The TAOMRR with its unique design and tunable characteristics can contribute to the development of next generation of optical communication technologies.

The TAOMRR architecture with five directional couplers is optimized and modeled utilizing delay line signal process method using Mason's gain rule. The unit delay is determined as [17]:

$$T = \frac{L_u n_g}{c} \tag{1}$$

where *Lu* is the minimal possible path known as unit delay length, *ng* is referred as refractive indices of the group, and *c* is the speed of light.

The FSR and unit delay have the following relation, which are defined as:

$$FSR = \frac{1}{T} = \frac{c}{L_{ug}} \tag{2}$$

From Equation (2), it clearly shows that unit delay length of the ring is inversely proportion to the FSR, i.e., ring radius reduction will result in increased FSR but this is limited till the bending loss did not become significant.

Group refractive indices are reliant on the efficient refractive indices along with centered frequencies. The relation is conveyed by Equation (3) [18]:

$$n_g = n_{eff} + f_o \left(dn_{eff}/df \right)_{f_o} \tag{3}$$

where "*neff*" stands for effectual refractive indices, and "*fo*" is a centered frequency.

Each and every ring perimeter is established in the following way in order to be an intrinsic multiple factor of the unit delay length. As a result, the microring perimeter is described by periodic multiples of unit delay length. In order to increase the entire FSR of TAOMRR, Vernier rule is introduced in the present work [19]:

$$FSR_{\text{overall}} = M{*}FSR_1 = N{*}FSR_2 = P{*}FSR_3 \tag{4}$$

where the coprime numbers of smaller, medium, and biggest ring, accordingly, are *M*, *N,* and *P,* whereas FSR1 represents the FSR of smaller ring, FSR2 represents the FSR of second larger ring, and FSR3 represents the FSR of larger ring. The overall FSR can be specified using the following relation [20]:

$$FSR = |M - N| \frac{(FSR_1 * FSR_2)}{|FSR_1 - FSR_2|} \tag{5}$$

Where:

$FSR_i = \frac{C}{2\pi n R_i}$, where $i = 1, 2, 3$.

2. Mathematical Modeling

The optical coupling is a unique method of connections between photonic signals when the two optical signals are appropriately closer to one another such that their momentary regions got overlapped with one another. A schematic illustration of specific optical coupling is presented in Figure 1.

Figure 1
Schematic diagram of directional optical coupler

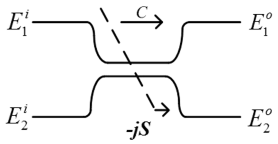

where E_1^i, E_2^i are the input fields, E_1^o, E_2^o are the field accumulated at the outputs where "*C*" and "*S*" are ports via coupling parameter as well as crossover port coupling coefficients, which is expressed as [18]:

$$C = \sqrt{1 - k} \tag{6}$$

$$-jS = -j\sqrt{k} \tag{7}$$

where "*k*" is a ratio of power coupling, which can be expressed as [5]:

$$k = \frac{P_{coupled}}{P_{input}} \tag{8}$$

where P_{coupled} is a coupling power through each single couplers, and P_{input} is the input power of the equivalent couplers. The directional optimal coupler is characterized in the block diagram form, which is presented in Figure 2.

Figure 2
A block representation of optical coupler

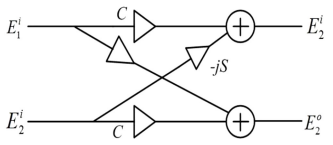

When the input and output fields are combined with the transmission matrix, it is represented as Equation (9).

$$\begin{bmatrix} E_1^0 \\ E_2^0 \end{bmatrix} = q \begin{bmatrix} C & -jS \\ -jS & C \end{bmatrix} \begin{bmatrix} E_1^i \\ E_2^i \end{bmatrix} \tag{9}$$

where "*q*" ($0 < q < 1$) is the coefficient of the magnitude in communications.

3. Transfer Function of the TAOMRR

The specified transmission parameter of a proposed TAOMRR is determined utilizing the signal flow graph method in the z-domain. Mason's gain formula is used in accordance with the following relationship below [21]:

$$T_f = \frac{\sum T_n \Delta_n}{\Delta} \tag{10}$$

where *Tn* is the transmission function of the forward direction, nth is a pathway from a determined input to a particular output port, Δ is a graph determined portion that concludes closed loop progression and correlative transmission across non-touching loops, and Δ*n* is an element that is equivalent to the sympathetic path essential with all the close loop in a continuous representation which is confined from forward direction under consideration. Value of Δ can be expressed as

$$\Delta = 1 - \sum L_a + \sum L_b - \sum L_c \ldots\ldots\ldots \tag{11}$$

where ΣL_a is a summation of all the each individual loops, ΣL_b is a summation of products of all accessible pair of two non-touching loops, and ΣL_c is the sum of product of all accessible pairs of three non-touching loops.

All the forward direction in addition to their route factors is discussed in Appendix.

Figure 3 illustrates the proposed TAOMRR where two smaller unsymmetrical microring are inserted diagonally inside a large microring. Figure 4 illustrates signal flow graph of a proposed arrangements in z-domain in addition to all the directional couplers in which $X(z)$ is expressed as the input signals and $Y(z)$ is expressed as the output signals.

The entire transmission function can be exhibited through Mason's rule, and it can be expressed by Equation (12).

Figure 3
The proposed arrangement of triple micro optical ring resonator

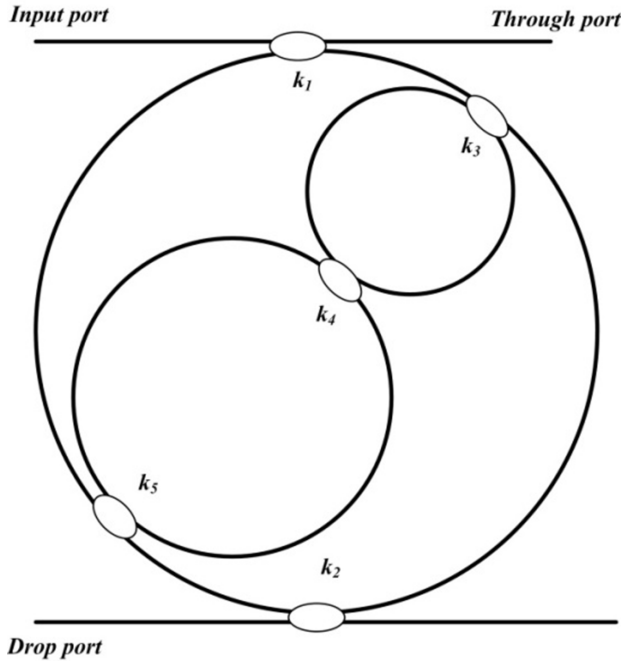

Figure 4
Transform-based schematic arrangement of the proposed configuration

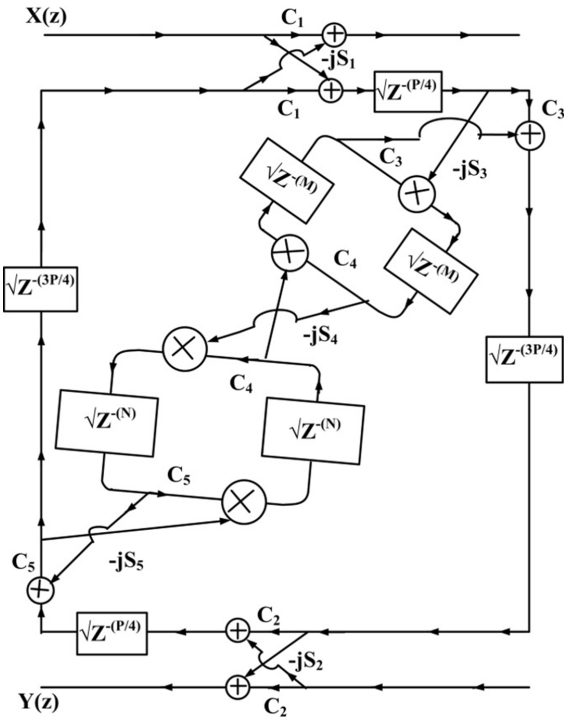

$$Tf = \frac{\begin{bmatrix} -C_3S_1S_2Z^{-\left(\frac{P}{2}\right)} + C_3^2C_4S_1S_2Z^{-\left(N+\frac{P}{2}\right)} + \\ C_3C_4C_5S_1S_2Z^{-\left(M+\frac{P}{2}\right)} - C_3^2C_5S_1S_2Z^{-\left(M+N+\frac{P}{2}\right)} \end{bmatrix}}{\begin{bmatrix} 1 - C_1C_2C_3C_5Z^{-(P)} - C_3C_4Z^{-(N)} - C_4C_5Z^{-(M)} + \\ C_1C_2C_3C_4C_5^2Z^{-(M+P)} + C_1C_2C_3^2C_4C_5Z^{-(N+P)} + \\ C_3C_5(C_4^2 + S_4^2)Z^{-(M+N)} - C_1C_2C_3^2C_5^2(C_4^2 + S_4^2)Z^{-(M+N+P)} \\ + jC_5S_3S_4S_5(C_1 + C_2)Z^{-\left(\frac{M}{2}+\frac{N}{2}+\frac{P}{2}\right)} \end{bmatrix}} \tag{12}$$

Considering the losses inside the rings, round trip bending loss can be expressed as $\{\gamma = \exp(-\alpha L)\}$ where 'α' is an average losses of the ring unit per length 'L' is length of ring and the propagating frequency coefficients (q), then Equation (12) will be altered as Equation (13) which is shown below:

$$\frac{\begin{bmatrix} -q^3\sqrt{\gamma_3}C_3S_1S_2Z^{-\left(\frac{P}{2}\right)} + q^5\gamma_2\sqrt{\gamma_3}C_3^2C_4S_1S_2Z^{-\left(N+\frac{P}{2}\right)} + \\ q^5\gamma_1\sqrt{\gamma_3}C_3C_4C_5S_1S_2Z^{-\left(M+\frac{P}{2}\right)} - q^5\gamma_1\gamma_2\sqrt{\gamma_3}C_3^2C_5S_1S_2Z^{-\left(M+N+\frac{P}{2}\right)} \end{bmatrix}}{\begin{bmatrix} 1 - q^4\sqrt{\gamma_3}\,C_1C_2C_3C_5Z^{-(P)} - q^2\gamma_2\,C_3C_4Z^{-(N)} - q^2\gamma_1\,C_4C_5Z^{-(M)} + \\ q^4\gamma_1\gamma_3C_1C_2C_3C_4C_5^2Z^{-(M+P)} + q^6\gamma_2\gamma_3\,C_1C_2C_3^2C_4C_5Z^{-(N+P)} + \\ q^4\gamma_1\gamma_2C_3C_5(C_4^2 + S_4^2)Z^{-(M+N)} - q^8\gamma_1\gamma_2\gamma_3C_1C_2C_3^2C_5^2(C_4^2 + S_4^2)Z^{-(M+N+P)} \\ + jq^5\sqrt{\gamma_1\gamma_2\gamma_3}C_5S_3S_4S_5(C_1 + C_2)Z^{-\left(\frac{M}{2}+\frac{N}{2}+\frac{P}{2}\right)} \end{bmatrix}} \tag{13}$$

The optimal transmittance circumstances are obtained by considering |Tf| of Equations (12) to one. By equating the equations mentioned above, it is conveyed as frequency domain $Z = \exp(j2\pi\nu T)$. Equation (12) can be significantly optimized by taking the exponential series to first order. The selection of $k2 = k3 = k4 = k5$ is taken to assess the directional couplers of optimal coupling coefficients. In resonance, the imaginary portion is zero. The correlation among $k1$ and $k2$ can be represented as

$$k_1 = 1 - \left[\frac{k_2 + (1 - k_2)k_2^{3/2}}{k_2(1 - k_2)^{3/2} - k_2\sqrt{k_2(1 - k_2)}} \right]^2 \quad (14)$$

The relationship between crosstalk and coupling coefficient is shown in Figure 5. The change in the crosstalk due to the change in $k1$ keeping $k2$ constant is shown in curve-1. At the meantime, curve-2 is considered from the change in crosstalk due to the change that $k2$ keeps $k1$ constant. The most effective coupling coefficient is obtained from the intersection of the two plots and is utilized to develop the proposed TAOMRR.

Figure 5
Coupling coefficient variation with crosstalk

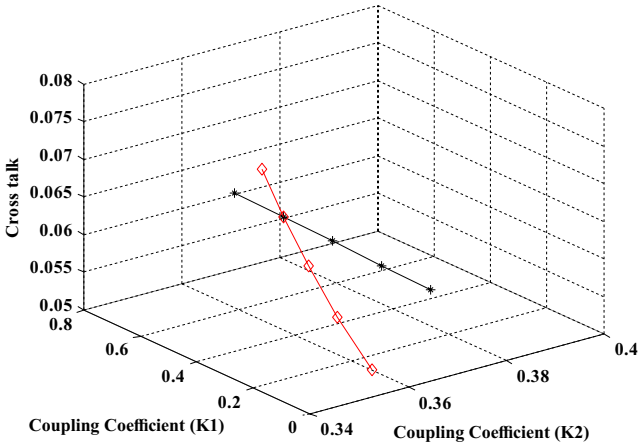

4. Characteristics of TAOMRR

In this paper, the following properties are analyzed using MATLAB.

1) Group delay

Group delay is the rate of change of negative phase angle derivative of transitions considering the frequency angle and can be mathematically expressed as [22]:

$$\tau_n = -\frac{d}{d\omega} \tan^{-1}\left[\frac{\mathrm{Im}\{H(z)\}}{\mathrm{Re}\{H(z)\}} \right]_{z=e^{j\omega}} \quad (15)$$

where $H(z)$ is a system frequency respond, and Im $\{H(z)\}$ and Re $\{H(z)\}$ are the imaginary and actual portion that suitably corresponds to the frequency feedback. Delay is the phase slope in which the amplitude is being determined.

2) Dispersion

This phenomenon is responsible for the derivative group delay depending on the frequency angle. The graphical representation of the signal distortion close to the resonance frequency is necessary because of dispersion. Dispersion of optical elements can be obtained by calibrating the group delay [23].

$$D = \frac{d(\tau_n)}{d\omega} \quad (16)$$

where ω is the angular frequency.

3) Finesse

The entire amount of round trips performed before the light intensity of microring resonator drops to the parameter of "e" is known as finesse. Mathematically, it can be suggested as the ratio of full width half maxima (FWHM) to the FSR and is expressed as F [24, 25]:

$$F = \frac{FSR}{FWHM} \quad (17)$$

4) Quality factor

The quality factor is also known as Q-factor. It is an essential property to design the sensors of microring resonator because it requires high frequency refinement. It is the ratio of energy exhausted per radian during resonance to energy stored in the resonator. It can be determined by calculating the FWHM and the centered frequency (f_o) [26].

$$Q = \frac{f_0}{FWHM} \quad (18)$$

When the coupling coefficients are very low (<1%), an extremely high quality factor can be established, but the output intensity will depreciate. The waveguide Q-factor can be improved by regulating the gap between the waveguide width and ring length [27].

5. FDTD Analysis of TAOMRR

Yee [28] introduced the FDTD in 1966 where the entire sequence of finite difference solutions is replaced in place of Maxwell equalization so that the time dependent for Maxwell's equations is directly solved:

$$-\mu_0 \frac{\partial H}{\partial t} = \nabla \times E \quad (19)$$

$$\varepsilon_0 \varepsilon_r \frac{\partial E}{\partial t} = \nabla \times H \quad (20)$$

In order to solve an EM complication, time and space can be used to discrete the waves. Initially, the FDTD was intended to work with electromagnetic waves which carried a wider bandwidth, such as microwaves. FDTD methodology is useful for numerous complex photonic configurations as it originates them into an upfront behavior. This is an extremely useful instrument for analyzing the field advancement of the ring resonator. The major advantage of FDTD accessibility is an overall reduction of similarities for the field light propagation shaped in its adequate amount and complexity. An additional substantial advantage is the wide range of material that can be accurately simulated in the context of FDTD [29, 30].

In this paper, using an OptiFDTD software, an effort is made to determine the field evolution of the arrangement of TAOMRR. The optimum coupling coefficient for directional couplers for the proposed TAOMRR was determined in MATLAB and designed using OptiFDTD software. OptiFDTD is used to develop each

optical directional coupler and the exhaustive layout is shown in Figure 6.

The arrangement consists of two asymmetric rings that are coupled with the larger ring diametrically. The height plot of the arrangement in OptiFDTD is shown in Figure 7. The DFT analysis of the height map of the amplitude field progression after the 2D simulation in the waveguides is shown in Figure 8. The DFT analysis of the image map of the amplitude field progression after the 2D simulation in the waveguides is shown in Figure 9.

Figure 6
Ring resonator layout in OptiFDTD with coupling gap and coupling coefficient obtained in MATLAB

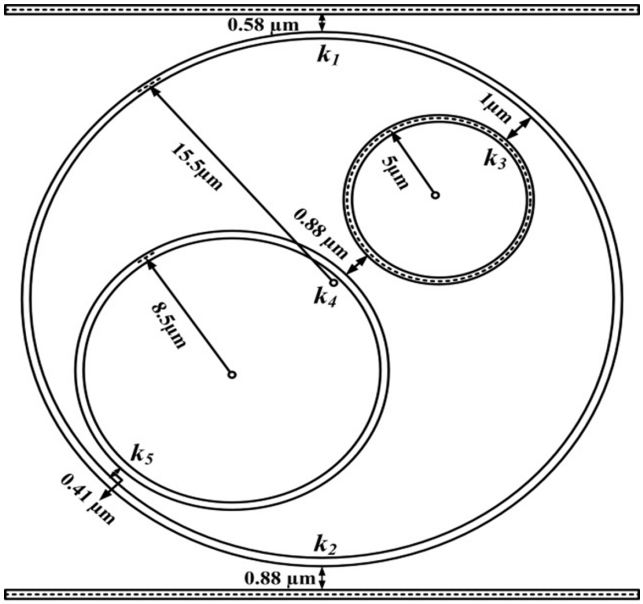

Waveguide Width= 570 nm
Waveguide Depth= 500 nm

Figure 7
3D representation of the resonator in OptiFDTD

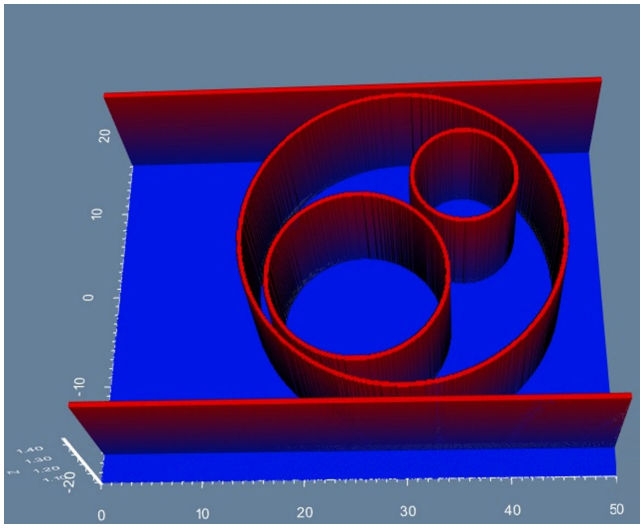

Figure 8
DFT analysis of field strength of amplitude height map along the waveguides of the proposed ring resonator in OptiFDTD where V and H are the electric field and magnetic field strength, respectively

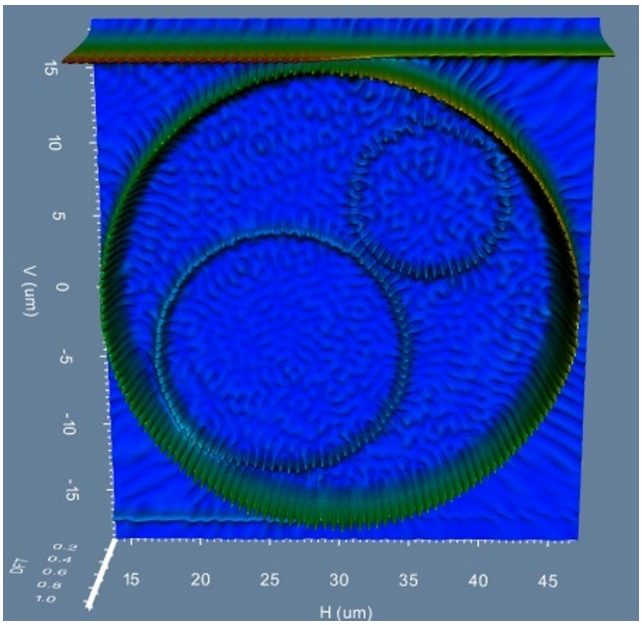

Figure 9
DFT analysis of field strength of amplitude image map (dB) along the waveguides of the determined ring resonator in OptiFDTD where V and H are the electric field and magnetic field strength, respectively

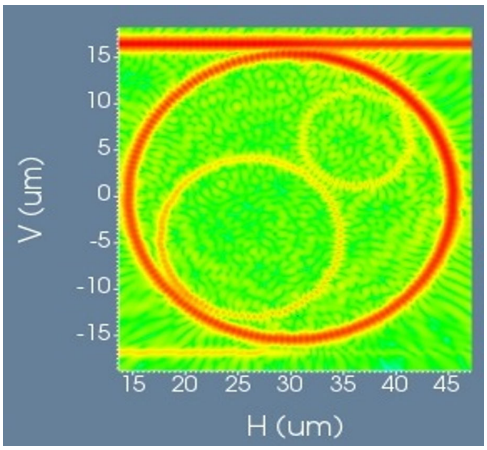

6. Simulation Results

Frequency responses evaluation of the reported TAOMRR is carried out in MATLAB software, and the field investigation is done utilizing OptiFDTD software. The optimal coupling factor determined in MATLAB software is $k1 = 0.4418$ and $k2 = k3 = k4 = k5 = 0.36$. Considering the wavelength core, the intrinsic refractive index is 2.0167 for silicon nitride (Si3N4) waveguides, the ring losses are chosen as 0.1 dB/cm, and transmitted coefficient frequency is assigned to 1. The width and depth for all considered waveguides (linear as well as ring waveguides) are

analyzed as 570 nm and 500 nm correspondingly. The rings perimeters are arranged in the ascending order of their size and preferred as 31.4160 μm, 53.4072 μm, and 97.3896 μm, which correlates with ring radius of 5.0 μm, 8.5 μm, and 15.5 μm consequently. The calculations are made to determine appropriate coprime resonant numbers as M = 10, N = 17, and P = 31.

The frequency response obtained from MATLAB simulation is shown in Figure 10 where the obtained FSR is found to be 21.65 THz. Again, the same attempt is made using OptiFDTD software, and then the response achieved is shown in Figure 11, which is very much in close agreement with what obtained from MATLAB simulation. The group delay and dispersion characteristic are shown in Figures 12 and 13, respectively, where it is clearly shown that the response is bulging around the resonant peaks. FWHM is an important characteristic for the calculation of finesse and Q-factor, which is shown in Figure 14. The obtained value of FWHM from Figure 14 is 90 GHz.

The input field specification contains a continuous wave with a center bandwidth of 1550 nm.

Figure 10
Frequency response plot in MATLAB

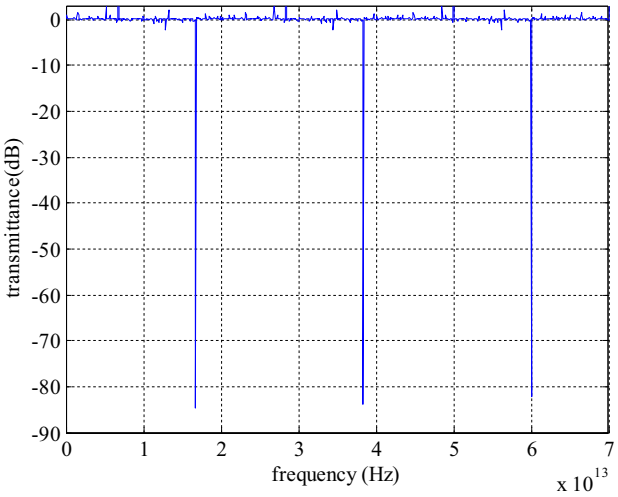

Figure 11
Frequency response plot in OptiFDTD

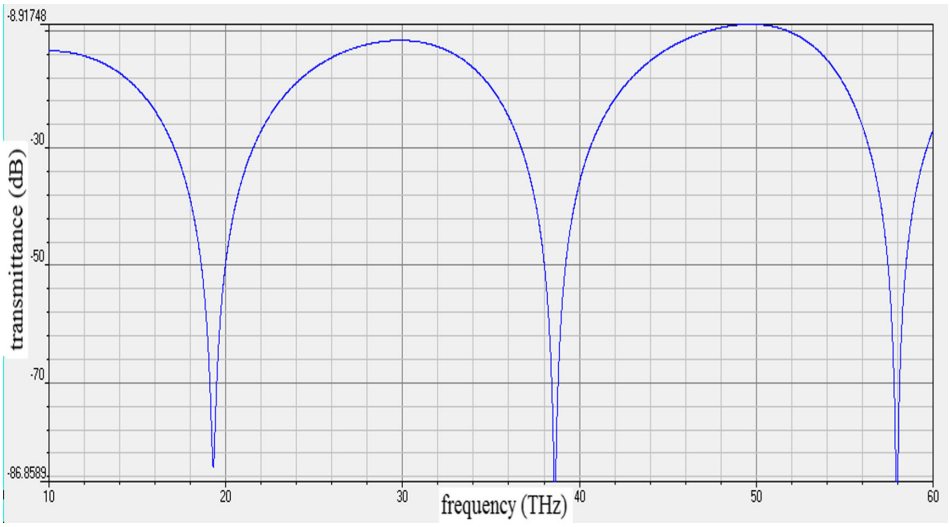

Figure 12
Group delay characteristics

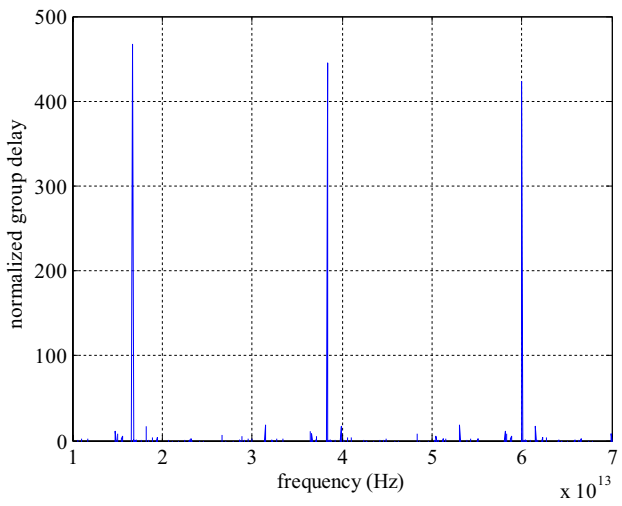

Figure 13
Dispersion characteristic

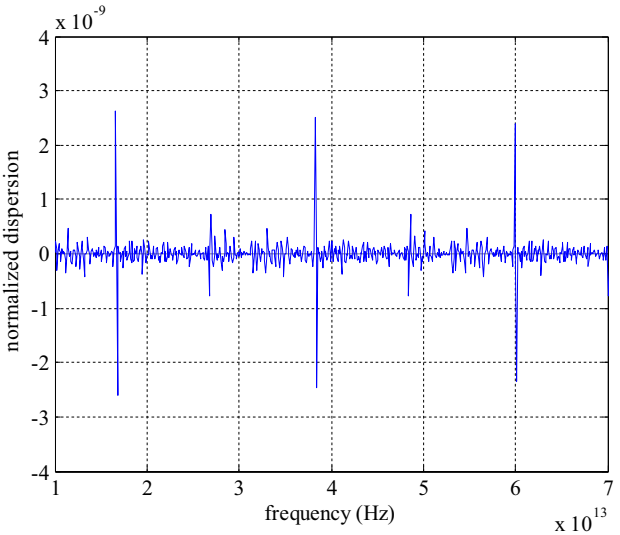

Figure 14
Finesse of the response

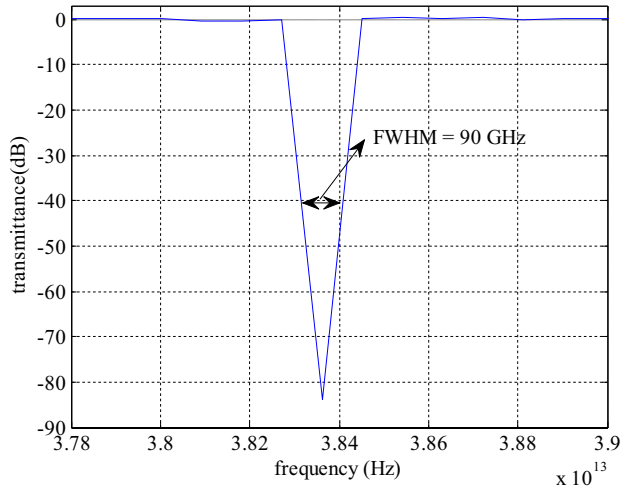

The frequency response obtained from OptiFDTD is in very close agreement with that obtained from MATLAB, i.e., the FSR obtained is around 21.65 THz. The shape of both plots depends on the operating principle of the software. In MATLAB, the frequency response of proposed configuration is achieved using codes, but in OptiFDTD the same response is not achieved using codes rather it is dependent on meshing, modes, etc. The objective is to achieve the desired bandwidth, which is same in both the plots.

7. Conclusion

The proposed TAOMRR is designed in z-domain utilizing delay line signal processing approach, and the Mason's gain rule is utilized to establish its transmission parameter. MATLAB software has been used to perform the simulation of proposed TAOMRR. The frequency response investigation is examined in MATLAB to obtain an FSR of 21.65 THz. Dispersion, group delay, and finesse properties are identified in MATLAB. The obtained finesse is 240.55. The OptiFDTD software is utilized to design the suggested configuration. The appropriate optical coupling for the proposed TAOMRR is designed using coupling coefficient from MATLAB. The frequency response obtained from OptiFDTD is in very close agreement with that obtained from MATLAB. The proposed method can perform performance investigation of unsymmetrical micro optical ring resonator and design its waveguide structure before actual fabrication.

Acknowledgments

The authors are very grateful to Director BIT Sindri, Jharkhand (Prof. Pankaj Rai) for his continuous support and motivation during entire period of this research.

Ethical Statement

This study does not contain any studies with human or animal subjects performed by any of the authors.

Conflicts of Interest

The authors declare that they have no conflicts of interest to this work.

Data Availability Statement

Data sharing is not applicable to this article as no new data were created or analyzed in this study.

Author Contribution Statement

Shree Krishna Marandi: Methodology, Software, Validation, Resources, Data curation. **Kumari Sarwagya:** Formal analysis, Investigation, Visualization, Project administration. **Suman Ranjan:** Conceptualization, Writing – original draft, Writing – review & editing, Supervision.

References

[1] Oda, K., Takato, N., & Toba, H. (1991). A wide-FSR waveguide double-ring resonator for optical FDM transmission systems. *Journal of Lightwave Technology*, *9*(6), 728–736. https://doi.org/10.1109/50.81975

[2] Ciminelli, C., Dell'Olio, F., Conteduca, D., Campanella, C. M., & Armenise, M. N. (2014). High performance SOI microring resonator for biochemical sensing. *Optics & Laser Technology*, *59*, 60–67. https://doi.org/10.1016/j.optlastec.2013.12.011

[3] Zangeneh-Nejad, F., & Safian, R. (2016). A graphene-based THz ring resonator for label-free sensing. *IEEE Sensors Journal*, *16*(11), 4338–4344. https://doi.org/10.1109/JSEN.2016.2548784

[4] Parimal, & Mandal, S. (2023). Design of an optical test bench (OTB) for an N-bit optical multiplier, optical convolution, and optical correlation circuit using an optical microring resonator in the Z-domain. *Optical and Quantum Electronics*, *55*(9), 844. https://doi.org/10.1007/s11082-023-04985-5

[5] Kisku, S., Sarwagya, K., & Ranjan, S. (2023). Performance investigation of triple unsymmetrical micro ring resonator as optical filter as well as biosensor. *Optical and Quantum Electronics*, *55*(2), 164. https://doi.org/10.1007/s11082-022-04443-8

[6] Garus, D., Hereth, R., & Schliep, F. (1994). Design considerations for Brillouin–Ringlaser gyroscopes. In *Conference Proceedings Symposium on Gyro Technology*, *2*, 2.

[7] Kalli, K., & Jackson, D. A. (1992). Ring resonator optical spectrum analyzer with 20-kHz resolution. *Optics Letters*, *17*(15), 1090–1092. https://doi.org/10.1364/OL.17.001090

[8] Suzuki, S., Oda, K., & Hibino, Y. (1995). Integrated-optic double-ring resonators with a wide free spectral range of 100 GHz. *Journal of Lightwave Technology*, *13*(8), 1766–1771. https://doi.org/10.1109/50.405322

[9] Moslehi, B., Goodman, J. W., Tur, M., & Shaw, H. J. (1984). Fiber-optic lattice signal processing. *Proceedings of the IEEE*, *72*(7), 909–930. https://doi.org/10.1109/PROC.1984.12948

[10] Jackson, K. P., Newton, S. A., Moslehi, B., Tur, M., Cutler, C. C., Goodman, J. W., & Shaw, H. J. (1985). Optical fiber delay-line signal processing. *IEEE Transactions on Microwave Theory and Techniques*, *33*(3), 193–210. https://doi.org/10.1109/TMTT.1985.1132981

[11] Mason, S. J. (1956). Feedback theory – Further properties of signal flow graphs. *Proceedings of the IRE*, *44*(7), 920–926. https://doi.org/10.1109/JRPROC.1956.275147

[12] Yanagase, Y., Suzuki, S., Kokubun, Y., & Chu, S. T. (2002). Box-like filter response and expansion of FSR by a vertically triple coupled microring resonator filter. *Journal of Lightwave Technology*, *20*(8), 1525–1529. https://doi.org/10.1109/JLT.2002.800296

[13] Kokubun, Y., Hatakeyama, Y., Ogata, M., Suzuki, S., & Zaizen, N. (2005). Fabrication technologies for vertically coupled microring resonator with multilevel crossing busline and ultracompact-ring radius. *IEEE Journal of Selected Topics in Quantum Electronics*, *11*(1), 4–10. https://doi.org/10.1109/JSTQE.2004.841720

[14] Yan, H., Feng, X., Zhang, D., & Huang, Y. (2013). Integrated optical add-drop multiplexer based on a compact parent-sub microring-resonator structure. *Optics Communications*, *289*, 53–59. https://doi.org/10.1016/j.optcom.2012.09.059

[15] Deng, L., Guo, X., Meng, Y., Zhao, T., Liu, Z., Xiao, H., . . . , & Yang, J. (2018). Demonstration of a microfiber-based add–drop filter using one tapered fiber. *IEEE Photonics Journal*, *10*(1), 1–6.

[16] Ahmed, R., Rifat, A. A., Yetisen, A. K., Salem, M. S., Yun, S. H., & Butt, H. (2016). Optical microring resonator based corrosion sensing. *RSC Advances*, *6*(61), 56127–56133. https://doi.org/10.1039/C6RA11538A

[17] Saeung, P., & Yupapin, P. P. (2008). Generalized analysis of multiple ring resonator filters: Modeling by using graphical approach. *Optik*, *119*(10), 465–472. https://doi.org/10.1016/j.ijleo.2006.12.017

[18] Madsen, C. K., & Zhao, J. H. (1999). Multi-stage AR architectures. In K. Chang, C. K. Madsen & J. H. Zhao (Eds.), *Optical filter design and analysis: A signal processing approach* (pp. 237–303). Wiley. https://doi.org/10.1002/0471213756.ch5

[19] Boeck, R., Shi, W., Chrostowski, L., & Jaeger, N. A. F. (2013). FSR-eliminated Vernier racetrack resonators using grating-assisted couplers. *IEEE Photonics Journal*, *5*(5), 2202511. https://doi.org/10.1109/JPHOT.2013.2280342

[20] Rabus, D. G. (2007). *Integrated ring resonators: The Compendium*. Germany: Springer.

[21] Nagrath, I. J. (2006). *Control systems engineering*. India: New Age International Publishers.

[22] Tavousi, A., Rakhshani, M. R., & Mansouri-Birjandi, M. A. (2018). High sensitivity label-free refractometer based biosensor applicable to glycated hemoglobin detection in human blood using all-circular photonic crystal ring resonators. *Optics Communications*, *429*, 166–174. https://doi.org/10.1016/j.optcom.2018.08.019

[23] Ranjan, S., & Mandal, S. (2018). Performance analysis of triple asymmetrical optical multiple ring resonator with a 1 × 3 input-output waveguide for application as an optical filter. *Applied Optics*, *57*(9), 2040–2049. https://doi.org/10.1364/AO.57.002040

[24] Gad, M., Ackert, J., Yevick, D., Chrostowski, L., & Jessop, P. (2011). Ring resonator wavelength division multiplexing interleaver. *Journal of Lightwave Technology*, *29*(14), 2102–2109. https://doi.org/10.1109/JLT.2011.2157081

[25] Ranjan, S., Sarwagya, K., Mandal, S., & Rai, P. (2021). Modelling and analysis of quadruple asymmetrical optical micro-ring resonator for biosensing application. *IEEE Sensors Journal*, *21*(18), 19904–19911. https://doi.org/10.1109/JSEN.2021.3096427

[26] Kajfez, D., Chebolu, S., Abdul-Gaffoor, M. R., & Kishk, A. A. (1999). Uncertainty analysis of the transmission-type measurement of Q-factor. *IEEE Transactions on Microwave Theory and Techniques*, *47*(3), 367–371. https://doi.org/10.1109/22.750244

[27] Menon, V. M., Tong, W., & Forrest, S. R. (2004). Control of quality factor and critical coupling in microring resonators through integration of a semiconductor optical amplifier. *IEEE Photonics Technology Letters*, *16*(5), 1343–1345. https://doi.org/10.1109/LPT.2004.826094

[28] Yee, K. (1966). Numerical solution of initial boundary value problems involving Maxwell's equations in isotropic media. *IEEE Transactions on Antennas and Propagation*, *14*(3), 302–307. https://doi.org/10.1109/TAP.1966.1138693

[29] Kedia, J., & Gupta, N. (2015). An FDTD analysis of serially coupled double ring resonator for DWDM. *Optik*, *126*(24), 5641–5644. https://doi.org/10.1016/j.ijleo.2015.09.031

[30] Sun, L., Yuan, J., Ma, T., Sang, X., Yan, B., Wang, K., & Yu, C. (2017). Design and optimization of silicon concentric dual-microring resonators for refractive index sensing. *Optics Communications*, *395*, 212–216. https://doi.org/10.1016/j.optcom.2016.05.052

How to Cite: Marandi, S. K., Sarwagya, K., & Ranjan, S. (2025). Triple Micro Optical Multiple Asymmetric Ring Resonator Performance Analysis as Optical Filter. *Journal of Optics and Photonics Research*, *2*(1), 45–53. https://doi.org/10.47852/bonviewJOPR42021793

Appendix

Single Loop

(1) $$L_1 = C_1C_2C_3C_5Z^{-(P)} \quad \text{(A.1)}$$

(2) $$L_2 = C_3C_4Z^{-(M)} \quad \text{(A.2)}$$

(3) $$L_3 = C_4C_5Z^{-(N)} \quad \text{(A.3)}$$

(4) $$L_4 = -C_3C_5S_4^2Z^{-(M+N)} \quad \text{(A.4)}$$

(5) $$L_5 = jC_2C_5S_3S_4S_5Z^{-\left(\frac{M}{2}+\frac{N}{2}+\frac{P}{2}\right)} \quad \text{(A.5)}$$

(6) $$L_6 = -jC_1C_5S_3S_4S_5Z^{-\left(\frac{M}{2}+\frac{N}{2}+\frac{P}{2}\right)} \quad \text{(A.6)}$$

Two Non-touching Loop

(7) $$L_{12} = C_1C_2C_3^2C_4C_5Z^{-(M+P)} \quad \text{(A.7)}$$

(8) $$L_{13} = C_1C_2C_3C_4C_5^2Z^{-(N+P)} \quad \text{(A.8)}$$

(9) $$L_{14} = -C_1C_2C_3^2C_5^2S_4^2Z^{-(M+N+P)} \quad \text{(A.9)}$$

(10) $$L_{23} = C_3C_4^2C_5Z^{-(M+N)} \quad \text{(A.10)}$$

Three Non-touching loop

(11) $$L_{123} = C_1C_2C_3^2C_4^2C_5^2Z^{-(M+N+P)} \quad \text{(A.11)}$$

Forward Path

(12) $$T_1 = -C_3S_1S_2Z^{-\left(\frac{P}{2}\right)} \quad \text{(A.12)}$$

Path Factor

(13) $$\Delta_1 = 1 - (L_2 + L_3 + L_4) + (L_{23}) \quad \text{(A.13)}$$

Determinant

(14) $$\Delta = 1 - (L_1 + L_2 + L_3 + L_4 + L_5 + L_6) + (L_{12} + L_{13} + L_{14} + L_{23}) - (L_{123}) \quad \text{(A.14)}$$